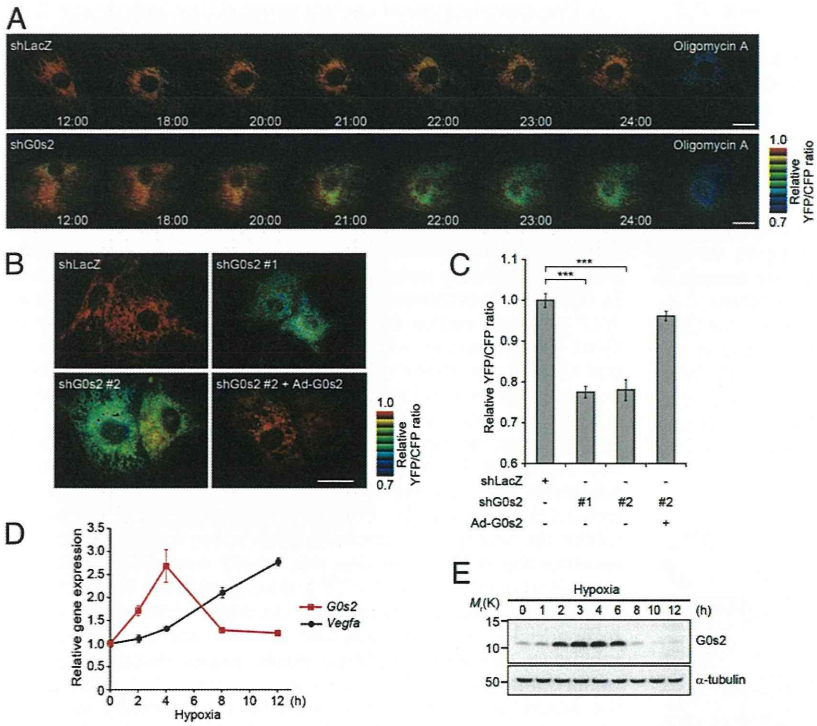

Fig. 2. G0s2, a hypoxia-inducible protein, affects intramitochondrial ATP concentration in cardiomyocytes. (*A*) Sequential YFP/CFP ratiometric pseudocolored images of Mit-ATeam fluorescence in cardiomyocytes expressing (*Upper*) shRNAs for LacZ (shLacZ) or (*Lower*) G0s2 (shG0s2). Oligomycin A (1 μg/mL) was added at the end of the time-lapse imaging to completely inhibit ATP synthesis. The indicated time represents the period after adenovirus infection. (*B*) Representative YFP/CFP ratiometric pseudocolored images of Mit-ATeam fluorescence in cardiomyocytes expressing the indicated adenovirus for 24 h. (Scale bar: *A* and *B*, 20 μm.) (*C*) The bar graph shows the mean YFP/CFP emission ratio of Mit-ATeam fluorescence in cardiomyocytes expressing shLacZ (n = 30), shG0s2 #1 (n = 30), shG0s2 #2 (n = 29), and shG0s2 #2 + G0s2 WT (n = 32) for 24 h. All of the measurements were normalized to the average of the control cells (shLacZ). ***$P < 0.001$. (*D*) Gene expression value plots of *G0s2* (red line) and *VEGF-α* (*Vegfa*; black line) levels in cardiomyocytes under hypoxic conditions (1% O_2). Each value was compared with the level of *Actb* expression (n = 3). Values represent the means ± SEMs. (*E*) Immunoblotting of the G0s2 expression in cardiomyocytes under hypoxic conditions (1% O_2).

expression that was induced during the cell cycle switch from G0 to G1 phase (18). G0s2 is expressed in many tissues and especially abundant in heart, skeletal muscle, liver, kidney, brain, and adipose tissue (19). Although G0s2 may play a role in cell cycle progression (20), the function of G0s2 in the hypoxic response remains unknown.

G0s2 Rescues the Decline of ATP Production During Hypoxia. We next tested whether the overexpression of the G0s2 before hypoxic stress could prevent hypoxia-induced ATP depletion. We prepared cardiomyocytes overexpressing G0s2 and control cardiomyocytes. During sustained hypoxia, $[ATP]_{mito}$ gradually declined in control cardiomyocytes as measured by the Mit-ATeam assay. Notably, the overexpression of G0s2 before the onset of hypoxia reduced this decline in $[ATP]_{mito}$, which allowed the cardiomyocytes to promptly recover to baseline levels of $[ATP]_{mito}$ after reoxygenation (Fig. 3 *A* and *B* and Movie S5). In addition, the prehypoxia overexpression of G0s2 preserved cell viability during sustained hypoxia (Fig. 3*C*). These results suggest that G0s2 can preserve mitochondrial ATP production even under hypoxia and protect cells from the energy crisis under hypoxia.

G0s2 Binds to F_oF_1-ATP Synthase but Not Other OXPHOS Protein Complexes. To reveal the mechanism by which G0s2 affects $[ATP]_{mito}$, we sought to identify the biochemical targets of G0s2. We screened for G0s2 binding proteins by immunoaffinity purification of cell lysates from cardiomyocytes expressing C-terminally Flag-tagged G0s2 (G0s2-Flag). G0s2-Flag is expressed in cardiomyocytes localized to the mitochondria (Fig. S4*A*). MS analysis revealed that multiple F_oF_1-ATP synthase subunits, but no other mitochondrial respiratory chain complex subunits, were coimmunoprecipitated with G0s2-Flag (Fig. S4*B* and Table S1). F_oF_1-ATP synthase is a well-known ATP-producing enzyme composed of a protein complex that contains an extramembranous F_1 and an intramembranous F_o domain linked by a peripheral and a central stalk (21–24). The binding of F_oF_1-ATP synthase to G0s2-Flag was confirmed by immunoblotting with antibodies against several subunits of F_oF_1-ATP synthase (Fig. 4*A*).

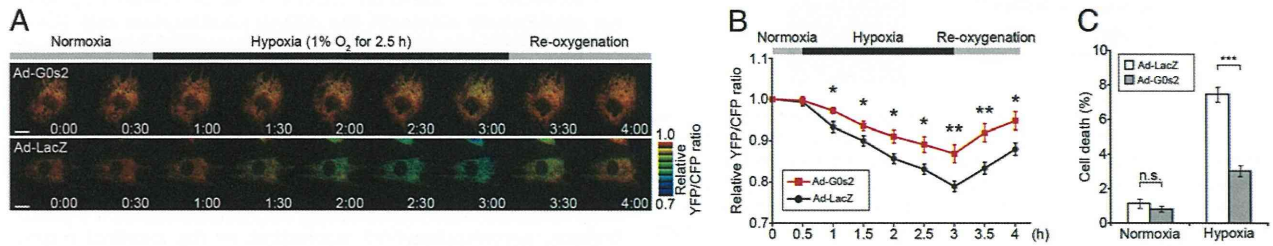

Fig. 3. Overexpression of G0s2 before hypoxia rescues the decline of mitochondrial ATP production during hypoxia. (*A*) Sequential YFP/CFP ratiometric pseudocolored images of Mit-ATeam fluorescence in cardiomyocytes expressing (*Upper*) G0s2 WT or (*Lower*) LacZ during hypoxia and reoxygenation. (Scale bar: 20 μm.) (*B*) YFP/CFP emission ratio plots of Mit-ATeam fluorescence in cardiomyocytes expressing G0s2 WT (n = 20) or LacZ (n = 19) during hypoxia and reoxygenation. All of the measurements were normalized to the ratio at time 0 and compared between cardiomyocytes with G0s2 WT and LacZ at each time point. (*C*) The bar graph shows the cell viability of cardiomyocytes overexpressing G0s2 under hypoxic conditions. Cardiomyocytes expressing either LacZ or G0s2 WT were cultured under normoxic or hypoxic conditions for 18 h (n = 8). The asterisks denote statistical significance comparing G0s2 with LacZ. Data are represented as the means ± SEMs. n.s., not significant. *$P < 0.05$; **$P < 0.01$; ***$P < 0.001$.

Conversely, G0s2-Flag was coimmunoprecipitated with F_oF_1-ATP synthase (Fig. S4*C*). G0s2-Flag was also found to be associated with the F_oF_1-ATP synthase in 293T and HeLa cells (Fig. S4*C*). Both coimmunoprecipitation using an anti-G0s2 antibody and a reciprocal immunoprecipitation revealed that endogenous G0s2 interacts with F_oF_1-ATP synthase, whereas none of the proteins in complexes I–IV or adenine nucleotide translocase 1 (ANT1; also referred to as ADP/ATP carrier) were coimmunoprecipitated with G0s2 (Fig. 4 *B* and *C*).

Given that the G0s2 protein contains an evolutionarily conserved amino terminus and one hydrophobic domain (HD) (19), we created three G0s2 partial deletion mutants to identify the domain in G0s2 that is important for binding to F_oF_1-ATP synthase (Fig. S4*D*). Among these mutants, G0s2 ΔC and G0s2 ΔN but not G0s2 ΔHD bound to the F_oF_1-ATP synthase complex (Fig. 4*D* and Fig. S4 *E* and *F*). Furthermore, we confirmed that G0s2 directly interacts with F_oF_1-ATP synthase in an in vitro pull-down assay using a recombinant maltose-binding protein–fused G0s2 protein and purified F_oF_1-ATP synthase from bovine heart mitochondria (Fig. S5). Immunocytochemical analysis revealed that endogenous G0s2 colocalized with the β-subunit of F_oF_1-ATP synthase (Fig. 4*E*). The knockdown of G0s2 expression by shRNA abolished G0s2 staining (Figs. S6 and S7*A*), indicating that both antibodies used for immunostaining specifically recognize G0s2. These data suggest that G0s2 interacts with the F_oF_1-ATP synthase complex through its HD in mitochondria and regulates OXPHOS activity.

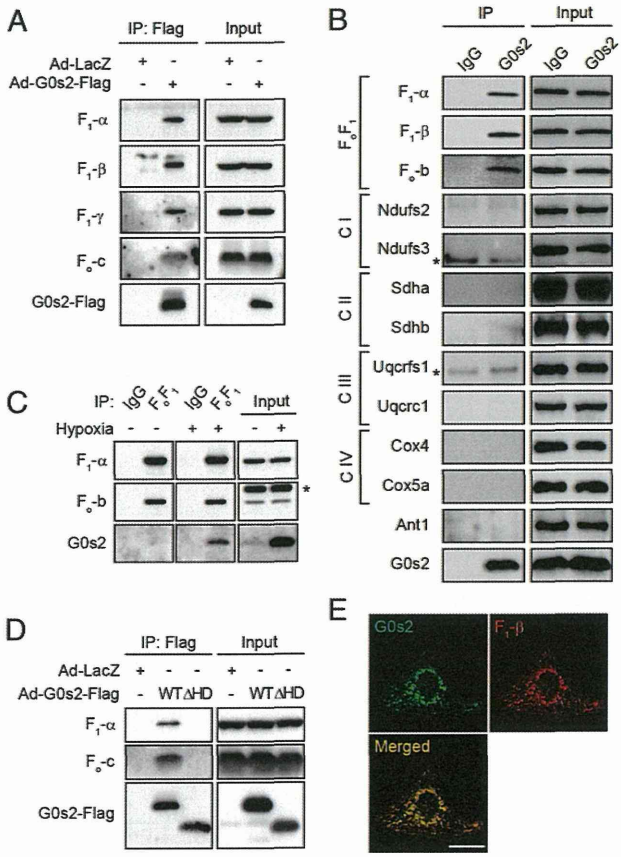

Fig. 4. G0s2 interacts with the F_oF_1-ATP synthase in mitochondria. (*A*) Immunoprecipitation (IP) of G0s2-Flag in cardiomyocytes. Cell lysates from cardiomyocytes expressing G0s2-Flag or LacZ were immunoprecipitated with an anti-Flag antibody. (*B*) IP of endogenous G0s2 in cardiomyocytes. Endogenous G0s2 was induced by hypoxia and immunoprecipitated using an anti-G0s2 antibody. C, OXPHOS complex; F_oF_1, F_oF_1-ATP synthase. *IgG light chain. (*C*) IP of F_oF_1-ATP synthase in cardiomyocytes under normoxic or hypoxic conditions. Cell lysates from cardiomyocytes cultured under normoxia or hypoxia for 4 h were immunoprecipitated with an antibody against the whole F_oF_1-ATP synthase complex or a control IgG. *Nonspecific band. (*D*) IP of G0s2 mutants expressed in cardiomyocytes. Cell lysates were immunoprecipitated with an anti-Flag antibody. (*E*) Immunostained images of hypoxia-stimulated (4 h) cardiomyocytes with anti-G0s2 (green) and anti–F_oF_1-ATP synthase β-subunit (red) antibodies. (Scale bars: 20 μm.)

G0s2 Increases Mitochondrial ATP Production Rate. $[ATP]_{mito}$ is mainly determined by the rate of ATP synthesis by F_oF_1-ATP synthase and ATP/ADP exchange by the ATP/ADP translocase ANT1. This theory means that the increased $[ATP]_{mito}$ observed in the G0s2-overexpressing cells may result from the increased ATP synthesis and/or decreased ATP/ADP exchange, although G0s2 did not interact with ANT1 (Fig. 4*B*). To resolve this issue and directly measure the rate of ATP production in mitochondria, we used a semiintact cell system called the mitochondrial activity of streptolysin O permeabilized cells (MASC) assay (25). In this assay, we permeabilized the plasma membrane to wash out any cytosolic components, such as creatine and glycolytic substrates, but left the mitochondria intact. Furthermore, we treated the cells with P^1, P^5-di(adenosine-5′) pentaphosphate to inhibit the activity of adenylate kinase. These steps allowed us to measure the ATP production rate mostly from OXPHOS, with a minimal contribution of ATP buffering systems in the cytosol. The MASC assay was suitable for accurate measurement of mitochondrial ATP production rate, because mitochondria in this semiintact cell system suffered much smaller damage than the isolated mitochondria in the conventional method. Surprisingly, in the MASC assay, the ATP production rate markedly increased when G0s2 was expressed in HeLa cells that lacked endogenous G0s2 (Fig. 5*A*). In cardiomyocytes, shRNA-mediated G0s2 knockdown decreased the ATP production rate in mitochondria, and the expression of G0s2 WT but not G0s2 ΔHD could restore the ATP production rate (Fig. 5*B* and Fig. S7*A*). In both cells, complete inhibition of ATP production by oligomycin A indicated that the observed ATP synthesis was catalyzed by OXPHOS but not other metabolism (Fig. 5 *A* and *B*).

Next, to evaluate the physiological role of G0s2, we examined whether endogenous G0s2 induced by hypoxia could enhance the ATP production rate. Cardiomyocytes were pretreated with hypoxia for 4 h, during which G0s2 expression was largely induced. We then evaluated the ATP production rate of both hypoxia-pretreated and nontreated cardiomyocytes under room air conditions. Even under these equivalent normoxic conditions, hypoxia-pretreated cardiomyocytes produced ATP faster than nontreated control cardiomyocytes (Fig. 5*C* and Fig. S7*B*). G0s2 knockdown attenuated this increase in the rate of ATP production, indicating that the enhanced ATP production rate resulting from hypoxia pretreatment primarily depends on endogenous G0s2 induction. This increased G0s2 expression was essential for cell survival, because G0s2-depleted cells died earlier than control cells under conditions of hypoxic stress (Fig. 5*D*)

Furthermore, to assess the effect of G0s2 on cellular respiration, we continuously measured the oxygen consumption rate (OCR) using an XF96 Extracellular Flux Analyzer. G0s2 knockdown decreased the basal OCR of cardiomyocytes, most likely because of the decreased activity of ATP synthesis (Fig. 5 *E* and *F*). In contrast, the proton leakage of the mitochondrial inner membrane and the maximum respiratory capacity of OXPHOS complexes I–IV were unaffected by G0s2 ablation (Fig. 5 *E* and *F*). These data show that G0s2 knockdown reduced respiration caused by ATP synthesis without affecting respiration caused by proton leakage, nonmitochondrial respiration, or the maximal respiration capacity.

All these findings indicate that G0s2 enhances the mitochondrial ATP production rate by increasing the activity of F_oF_1-ATP synthase.

Discussion

In this study, we showed that G0s2 kinetically increased OXPHOS activity through direct binding to F_oF_1-ATP synthase. Our previous

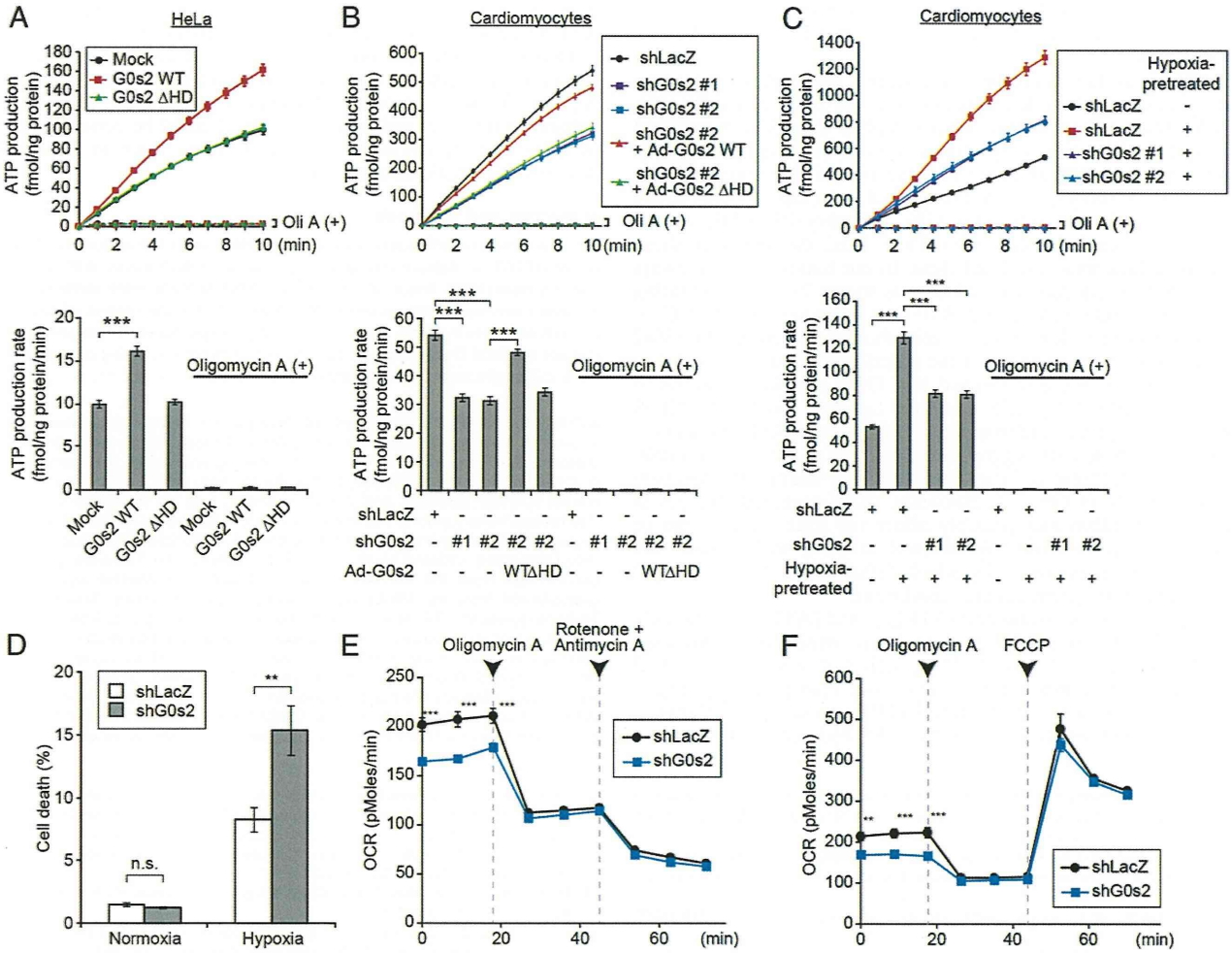

Fig. 5. G0s2 enhances the mitochondrial ATP production rate. (*A* and *B*) MASC assay of (*A*) permeabilized HeLa cells expressing the indicated plasmids or (*B*) cardiomyocytes expressing the indicated adenovirus in the presence (dotted lines) or absence (solid lines) of 1 μg/mL oligomycin A (Oli A). *Upper* shows the ATP production plots, and *Lower* shows the mean ATP production rates between 0 and 10 min. (*A*) $n = 12$. (*B*) Solid lines, $n = 12$; dotted lines, $n = 8$. (*C*) MASC assay of permeabilized cardiomyocytes pretreated with hypoxia. Cells expressing the indicated adenovirus were pretreated with or without hypoxia for 4 h. After the pretreatment, the cells were permeabilized under room air conditions followed by MASC assay in the presence (dotted lines; $n = 8$) or absence (solid lines; $n = 12$) of 1 μg/mL Oli A. *Upper* shows the ATP production plot, and *Lower* shows the mean ATP production rate between 0 and 10 min. (*D*) The bar graph represents the cell viability of G0s2-depleted cardiomyocytes under hypoxic conditions. Cardiomyocytes expressing shLacZ or shG0s2 (#2) were cultured under normoxic or hypoxic conditions for 18 h. (*E* and *F*) The OCR in cardiomyocytes expressing shLacZ and shG0s2 (#2) under basal conditions and in response to the indicated mitochondrial inhibitors ($n = 8$). FCCP, carbonyl cyanide-4-(trifluoromethoxy)-phenylhydrazone. Data are represented as the means ± SEMs. n.s., not significant. $^{**}P < 0.01$; $^{***}P < 0.001$.

studies of F_oF_1-ATP synthase have revealed that this enzyme has a specific structure that connects two molecular nanomotors that synchronize with each other to produce ATP (26–30). These physically distinct structures suggest that a specific activating factor for F_oF_1-ATP synthase must exist. Combined with the findings from this study, we hypothesize that G0s2 may lower the activation barrier of the F_oF_1-ATP synthase nanomotor and enhance the ATP production rate with the equivalent proton motive driving force (PMF; i.e., the sum of the membrane potential and the pH gradient). Activation barriers might be generated by various factors, such as friction between the stator and rotor of F_oF_1-ATP synthase, physical and electrical resistance to proton transport through the channel, and the existence of rotary blockers such as the bacterial ε-subunit and cyclophilin D (31). The increased ATP production rate caused by G0s2 overexpression observed in the MASC assay supports this hypothesis, because the PMF in the initial phase of this assay should be the same. If this hypothesis is true, even with reduced PMF, cells that express G0s2 should produce ATP faster than cells that express little or no G0s2. In fact, G0s2 overexpression attenuated the decline of $[ATP]_{mito}$ under hypoxic conditions that reduced the PMF. Precise real-time measurement of the PMF is currently difficult, but these hypotheses might be proven in future studies. Kinetically faster ATP production should accompany greater consumption of both O_2 and PMF; however, our results suggest that preserving ATP production is more beneficial than preserving PMF for cell viability, particularly when the O_2 supply is restricted but still exists. The transience of endogenous G0s2 expression induced by hypoxia might serve to protect tissues in the early phase of energy crisis. There may be specific mechanisms to decrease G0s2 expression under prolonged ischemia that have yet to be identified. Another possible mechanism by which G0s2 could increase the ATP production rate is that G0s2 increases the F_o-F_1 coupling efficiency of F_oF_1-ATP synthase. However, this hypothesis is less likely, because G0s2 altered the oxygen consumption rate to increase the ATP production rate. Although this uncoupling phenomenon has rarely been reported for mammalian mitochondrial F_oF_1-ATP synthase, we cannot completely eliminate the possibility that intrinsically

uncoupled F_oF_1-ATP synthase exists, because we could not accurately measure the amount of uncoupled F_oF_1-ATP synthase in intact cells.

G0s2 was first identified in cultured monocytes during the drug-induced cell cycle transition from G0 to G1 phase (18, 32). A limited number of studies have implied that G0s2 is involved in cell proliferation (33), differentiation (19), apoptosis (34), inflammation (35), and lipid metabolism (36) in various cellular settings. Moreover, G0s2 was reported to localize to the cytosol (33), endoplasmic reticulum (19), mitochondria (34), or the surface of lipid droplets (36). How G0s2 distinguishes these multiple functions is still not clear. In our hands, G0s2 is always localized to mitochondria, which was shown by immunostaining with two antibodies against different epitopes of G0s2 (Fig. S6). Complete depletion of mitochondrial staining by G0s2 knockdown strongly suggests the specific localization of G0s2 to mitochondria. We also showed that G0s2 specifically bound to mitochondrial F_oF_1-ATP synthase but not other OXPHOS protein complexes and functionally regulated OXPHOS activity. Together, these data suggest that G0s2 acts in the mitochondria. However, different cellular conditions may change the localization and role of G0s2. Additionally, G0s2-mediated changes in ATP metabolism may possibly affect the lipid metabolism or cellular proliferation. Additional studies will reveal the functional mechanisms by which G0s2 exerts these multiple functions in different cellular conditions.

In this study, we evaluated $[ATP]_{mito}$ and $[ATP]_{cyto}$ separately using FRET-based ATP biosensors in living cells. This dual evaluation revealed that $[ATP]_{mito}$ reflected mitochondrial ATP production with much greater sensitivity than $[ATP]_{cyto}$ (Fig. 1 and Movies S1 and S2). Because $[ATP]_{cyto}$ is strongly influenced by the activity of various cytosolic ATP hydrolytic enzymes and ATP buffering enzymes, $[ATP]_{cyto}$ does not always reflect the ATP availability that determines cellular function.

Taken together, our results indicate that G0s2 is a positive regulator of OXPHOS that works to increase the mitochondrial ATP production rate even under hypoxic conditions. Therefore, enhancing the level and function of G0s2 could be beneficial for hypoxia- and mitochondria-related disorders, such as ischemic diseases, metabolic diseases, and cancer.

Materials and Methods

Cells were infected with adenovirus encoding FRET-based ATP indicators AT1.03 or mit-AT1.03 to measure changes in cytosolic or mitochondrial ATP concentrations, respectively. Image acquisitions and FRET analyses were performed as described previously with some modifications (13). For the control of oxygen concentration during time-lapse imaging, digital gas mixer for stage-top incubator GM8000 (Tokai Hit) was used to create hypoxic (1% O_2) or normoxic (20% O_2) condition. Additional methods are found in *SI Materials and Methods*.

ACKNOWLEDGMENTS. We thank M. Murata for helpful discussions and advice, H. Miyagi (Olympus Co. Ltd.) for technical advice regarding microscopy, T. Miyazaki (Cyclex Co. Ltd.) for making antibodies, S. Ikezawa and A. Ogai for technical assistance, K. Tanaka for help with the purification of bovine F_oF_1-ATP synthase, and Y. Okada and H. Fujii for secretarial support. This research was supported by the Japan Society for the Promotion of Science through the Funding Program for Next Generation World-Leading Researchers (NEXT Program) initiated by the Council for Science and Technology Policy; grants-in-aid from the Ministry of Health, Labor, and Welfare–Japan; and grants-in-aid from the Ministry of Education, Culture, Sports, Science, and Technology–Japan. This research was also supported by grants from Takeda Science Foundation, Japan Heart Foundation, Japan Cardiovascular Research Foundation, Japan Intractable Diseases Research Foundation, Japan Foundation of Applied Enzymology, Japan Medical Association, Uehara Memorial Foundation, Mochida Memorial Foundation, Banyu Foundation, Naito Foundation, Inoue Foundation for Science, Osaka Medical Research foundation for Intractable Diseases, Ichiro Kanehara Foundation, and Showa Houkoukai.

1. Kim JW, Tchernyshyov I, Semenza GL, Dang CV (2006) HIF-1-mediated expression of pyruvate dehydrogenase kinase: A metabolic switch required for cellular adaptation to hypoxia. *Cell Metab* 3(3):177–185.
2. Papandreou I, Cairns RA, Fontana L, Lim AL, Denko NC (2006) HIF-1 mediates adaptation to hypoxia by actively downregulating mitochondrial oxygen consumption. *Cell Metab* 3(3): 187–197.
3. Semenza GL (2012) Hypoxia-inducible factors in physiology and medicine. *Cell* 148(3): 399–408.
4. Semenza GL, et al. (1996) Hypoxia response elements in the aldolase A, enolase 1, and lactate dehydrogenase A gene promoters contain essential binding sites for hypoxia-inducible factor 1. *J Biol Chem* 271(51):32529–32537.
5. Chen YC, et al. (2012) Identification of a protein mediating respiratory supercomplex stability. *Cell Metab* 15(3):348–360.
6. Fukuda R, et al. (2007) HIF-1 regulates cytochrome oxidase subunits to optimize efficiency of respiration in hypoxic cells. *Cell* 129(1):111–122.
7. Strogolova V, Furness A, Robb-McGrath M, Garlich J, Stuart RA (2012) Rcf1 and Rcf2, members of the hypoxia-induced gene 1 protein family, are critical components of the mitochondrial cytochrome bc1-cytochrome c oxidase supercomplex. *Mol Cell Biol* 32(8):1363–1373.
8. Saks V, et al. (2006) Cardiac system bioenergetics: Metabolic basis of the Frank-Starling law. *J Physiol* 571(Pt 2):253–273.
9. Smolenski RT, Lachno DR, Ledingham SJ, Yacoub MH (1990) Determination of sixteen nucleotides, nucleosides and bases using high-performance liquid chromatography and its application to the study of purine metabolism in hearts for transplantation. *J Chromatogr A* 527(2):414–420.
10. Shimura D, et al. (2013) Metabolomic profiling analysis reveals chamber-dependent metabolite patterns in the mouse heart. *Am J Physiol Heart Circ Physiol* 305(4):H494–H505.
11. Kemp GJ, Meyerspeer M, Moser E (2007) Absolute quantification of phosphorus metabolite concentrations in human muscle in vivo by 31P MRS: A quantitative review. *NMR Biomed* 20(6):555–565.
12. Ford SR, et al. (1996) Use of firefly luciferase for ATP measurement: Other nucleotides enhance turnover. *J Biolumin Chemilumin* 11(3):149–167.
13. Imamura H, et al. (2009) Visualization of ATP levels inside single living cells with fluorescence resonance energy transfer-based genetically encoded indicators. *Proc Natl Acad Sci USA* 106(37):15651–15656.
14. Lopaschuk GD, Kelly DP (2008) Signalling in cardiac metabolism. *Cardiovasc Res* 79(2): 205–207.
15. Hattori F, et al. (2010) Nongenetic method for purifying stem cell-derived cardiomyocytes. *Nat Methods* 7(1):61–66.
16. Forsythe JA, et al. (1996) Activation of vascular endothelial growth factor gene transcription by hypoxia-inducible factor 1. *Mol Cell Biol* 16(9):4604–4613.
17. Wolf A, et al. (2011) Hexokinase 2 is a key mediator of aerobic glycolysis and promotes tumor growth in human glioblastoma multiforme. *J Exp Med* 208(2):313–326.
18. Russell L, Forsdyke DR (1991) A human putative lymphocyte G0/G1 switch gene containing a CpG-rich island encodes a small basic protein with the potential to be phosphorylated. *DNA Cell Biol* 10(8):581–591.
19. Zandbergen F, et al. (2005) The G0/G1 switch gene 2 is a novel PPAR target gene. *Biochem J* 392(Pt 2):313–324.
20. Heckmann BL, Zhang X, Xie X, Liu J (2013) The G0/G1 switch gene 2 (G0S2): Regulating metabolism and beyond. *Biochim Biophys Acta* 1831(2):276–281.
21. Dimroth P, von Ballmoos C, Meier T (2006) Catalytic and mechanical cycles in F-ATP synthases. Fourth in the Cycles Review Series. *EMBO Rep* 7(3):276–282.
22. Senior AE (2007) ATP synthase: Motoring to the finish line. *Cell* 130(2):220–221.
23. Walker JE (1998) ATP synthesis by rotary catalysis (Nobel Lecture). *Angew Chem Int Ed* 37:5000–5011.
24. Yoshida M, Muneyuki E, Hisabori T (2001) ATP synthase—a marvellous rotary engine of the cell. *Nat Rev Mol Cell Biol* 2(9):669–677.
25. Fujikawa M, Yoshida M (2010) A sensitive, simple assay of mitochondrial ATP synthesis of cultured mammalian cells suitable for high-throughput analysis. *Biochem Biophys Res Commun* 401(4):538–543.
26. Adachi K, et al. (2007) Coupling of rotation and catalysis in F(1)-ATPase revealed by single-molecule imaging and manipulation. *Cell* 130(2):309–321.
27. Itoh H, et al. (2004) Mechanically driven ATP synthesis by F1-ATPase. *Nature* 427(6973):465–468.
28. Noji H, Yasuda R, Yoshida M, Kinosita K, Jr. (1997) Direct observation of the rotation of F1-ATPase. *Nature* 386(6622):299–302.
29. Rondelez Y, et al. (2005) Highly coupled ATP synthesis by F1-ATPase single molecules. *Nature* 433(7027):773–777.
30. Uchihashi T, Iino R, Ando T, Noji H (2011) High-speed atomic force microscopy reveals rotary catalysis of rotorless F_1-ATPase. *Science* 333(6043):755–758.
31. Giorgio V, et al. (2009) Cyclophilin D modulates mitochondrial F0F1-ATP synthase by interacting with the lateral stalk of the complex. *J Biol Chem* 284(49):33982–33988.
32. Siderovski DP, Blum S, Forsdyke RE, Forsdyke DR (1990) A set of human putative lymphocyte G0/G1 switch genes includes genes homologous to rodent cytokine and zinc finger protein-encoding genes. *DNA Cell Biol* 9(8):579–587.
33. Yamada T, Park CS, Burns A, Nakada D, Lacorazza HD (2012) The cytosolic protein G0S2 maintains quiescence in hematopoietic stem cells. *PLoS ONE* 7(5):e38280.
34. Welch C, et al. (2009) Identification of a protein, G0S2, that lacks Bcl-2 homology domains and interacts with and antagonizes Bcl-2. *Cancer Res* 69(17):6782–6789.
35. Kobayashi S, et al. (2008) Expression profiling of PBMC-based diagnostic gene markers isolated from vasculitis patients. *DNA Res* 15(4):253–265.
36. Yang X, et al. (2010) The G(0)/G(1) switch gene 2 regulates adipose lipolysis through association with adipose triglyceride lipase. *Cell Metab* 11(3):194–205.

Supporting Information

Kioka et al. 10.1073/pnas.1318547111

SI Materials and Methods

Reagents and Antibodies. Reagents in the report were purchased as follows: oligomycin A (Sigma-Aldrich), 2-deoxyglucose (Sigma-Aldrich), and Mitotracker Red (Invitrogen). Antibodies were purchased as follows: anti–F_oF_1-ATP synthase complex (complex V; MitoSciences); anti–F_oF_1-ATP synthase subunits F_1-α (Proteintech), F_1-β (Invitrogen), F_1-γ (Abcam), and F_o-b (Proteintech); Ndufs2 (Abcam); Ndufs3 (Abcam); Sdha (Abcam); Sdhb (Abcam); Uqcrfs1 (Abcam); Uqcrc1 (Abcam); Cox4 (Abcam); Cox5a (Abcam); adenine nucleotide translocase 1 (Abcam); anti–α-tubulin (Sigma-Aldrich); anti-Flag M2 (Sigma-Aldrich); HRP-coupled sheep anti-rabbit and anti-mouse IgG (Cappel); and Alexa 488- and Alexa 568-labeled secondary antibodies (Invitrogen). Anti–F_oF_1-ATP synthase c subunit antibody is generated by immunization with peptide corresponding to human c subunit. Polyclonal antibodies against G0/G1 switch gene 2 (G0s2) were generated by immunization with peptide corresponding to mouse G0s2 amino acid sequence (amino acids 93–103, CSRALSLRQHAS or amino acids 49–103, PFTAASRLRDQEAAVVELREACEQQSLHKQALLAGGKAQEATLCSRALSLRQHAS) in rabbit. Monoclonal antibody against G0s2 was generated by immunization with peptide corresponding to mouse G0s2 amino acid sequence (amino acids 93–103) in mouse.

Cell Culture and Transfection. Cardiomyocytes obtained from 1- or 2-d-old Wister rats were prepared and cultured in DMEM (Invitrogen) containing 10%(vol/vol) FBS as described previously (1). Hypoxic condition (1% O_2) was provided by MCO-5M multigas incubator (Sanyo) unless described otherwise. HeLa and 293T cells were maintained in DMEM containing 10% FBS and 1% penicillin streptomycin. Transient transfection was performed using FuGENE 6 (Promega) for HeLa or Lipofectamine 2000 (Invitrogen) for 293T cells.

Constructs. The coding sequence of mouse G0s2 gene (NM_008059.3) was amplified by PCR from mouse heart cDNA library and subcloned into pENTR/D-TOPO (Invitrogen) (pENTR-G0s2) using Gateway Technology. The deletion mutants of N-terminal, hydrophobic domain (HD), and C-terminal portions of G0s2 (ΔN, ΔHD, and ΔC, respectively) were generated by PCR using pENTR-G0s2 as a template. The pENTR-G0s2 clones were recombined into pEF-DEST51/Flag, generating C-terminally Flag-tagged G0s2 (G0s2-Flag). For adenoviral construction, we used ViraPower Adenoviral Expression System (Invitrogen) for overexpression and BLOCK-iT Adenoviral RNAi Expression System for shRNA (Invitrogen) according to the manufacturer's instructions. For shRNA construction, oligonucleotides containing the target sequence were subcloned into pENTR-U6 and recombined into pAd/BLOCK-iT-DEST. The targets of shRNA for G0s2 (#1) and (#2) are the coding region and 3′-UTR of rat G0s2, respectively. The used sequences are as follows:

shRNA for G0s2 (#1), GGAAGCTAGTGAAGCTGTACG;

shRNA for G0s2 (#2), GCAGCATGCACTGTGATTTGT; and

shRNA for LacZ, GCTACACAAATCAGCGATTT.

RNA Extraction and Quantitative RT-PCR. Total RNA was extracted from cardiomyocytes using RNA-Bee Reagent (Tel-Test) and converted to cDNA using the Omniscript RT Kit (Qiagen) according to the manufacturer's instructions. Quantitative RT-PCR was performed with TaqMan technology and StepOnePlus Real-Time PCR Systems (Applied Biosystems). All of the samples were processed in duplicate. The level of each transcript was quantified by the threshold cycle method using *Actb* as an endogenous control.

Hybridization to Oligonucleotide Arrays. cDNA was synthesized from total RNA and annealed to a T7-oligo-dT primer. Reverse transcription was done with SuperScript II reverse transcriptase. Second-strand cDNA synthesis was done with DNA polymerase I with the appropriate reagents. Synthesis of biotin-labeled cRNA was done by in vitro transcription with the MEGAscript T7 IVT Kit (Ambion). The cRNA was fragmented and hybridized to GeneChip Rat Genome 230 2.0 arrays (Affymetrix). Hybridization, probe washing, staining, and probe array scan were done according to the manufacturer's instructions.

Microarray Data Analysis. Data analysis and normalization were performed by GeneSpring Gx11.5 bioinformatics software (Agilent Technologies), excluding the probe sets with raw signal (<50) in all arrays. After applying quality filtering to diminish background noise created by nonsignificant gene probes, one-way ANOVA test was applied to the filtered gene list, resulting in a group of genes with significant P values. Heat maps were generated by GeneSpring Gx11.5.

Purification of G0s2 Binding Protein. Cardiomyocytes were lysed with CHAPS lysis buffer of 30 mM Mops, pH 7.5, 150 mM NaCl, 10%(vol/vol) glycerol, 1 mM EDTA, 10 mM NaF, 25 mM β-glycerophosphate, 1 mM orthovanadate, 1% CHAPS, and protease inhibitor mixture (Nacalai-tesque). The lysates were immunoprecipitated with anti-Flag M2-agarose (Sigma-Aldrich) at 4 °C for 1 h. After extensive washing, the proteins were eluted with 250 μg/mL Flag peptide. The eluate was electrophoresed on 4–12% NuPAGE Bis·Tris gel and stained with silver. Gel pieces, including specific bands from the silver-stained gels, were excised, digested with trypsin, and analyzed with Q-TOF tandem mass spectrometer SYNAPT G2 (Waters).

Immunoprecipitation. Cells were lysed with CHAPS lysis buffer as described above. For immunoprecipitation of endogenous G0s2, the cell lysates underwent the two preclear steps: protein G-Sepharose (GE Healthcare) for 30 min followed by anti-rabbit IgG plus Dynabeads M-280 anti-rabbit IgG (Invitrogen) for 30 min at 4 °C. The precleared samples were immunoprecipitated with anti-G0s2 antibody and Dynabeads M-280 anti-rabbit IgG for 2 h at 4 °C. For immunoprecipitation of F_oF_1-ATP synthase, the cell lysates were immunoprecipitated with anti–F_oF_1-ATP synthase complex antibody and Dynabeads M-280 anti-mouse IgG (Invitrogen) overnight at 4 °C without a preclear step. After washing, the bound proteins were eluted with SDS/PAGE sample buffer.

FRET-Based Measurement of Mitochondrial Matrix and Cytosolic ATP Concentration. Cardiomyocytes were infected with adenovirus encoding FRET-based ATP indicators AT1.03 or mit-AT1.03 to measure changes in cytosolic or mitochondrial ATP concentrations, respectively. Wide-field observations of the cells were performed on an Olympus IX-81 inverted fluorescence microscope (Olympus) using a PL APO 60X, 1.35 N.A., oil immersion objective lens (Olympus). Fluorescence emission from ATP indicator based on ε-subunit for analytical measurements (ATeam) was imaged by using a dual cooled CCD camera (ORCA-D2; Hamamatsu Photonics) with a dichroic mirror (510 nm) and two

emission filters (483/32 nm for CFP and 542/27 nm for YFP; A11400-03; Hamamatsu Photonics). Cells were illuminated using the CoolLED *p*E-1 excitation system (CoolLED) with a wavelength of 425 nm. Cells were maintained on a microscope at 37 °C using a stage-top incubator (Tokai Hit). For the control of oxygen concentration during time-lapse imaging, a digital gas mixer for stage-top incubator GM8000 (Tokai Hit) was used to create hypoxic (1% O_2) and normoxic (20% O_2) conditions. A laser-based Z drift compensator (IX81-ZDC; Olympus) was used to minimize the focus drift during the time-lapse imaging. Image analysis was performed using MetaMorph (Molecular Devices). The YFP/CFP emission ratio was calculated by dividing pixel by pixel a YFP image with a CFP image after background subtraction.

Confocal Microscopy. After treated with 50 nM Mitotracker Red for 4 h, cardiomyocytes were fixed with 100% methanol for 15 min at −20 °C, permeabilized with 0.01% Triton X-100 in PBS at room temperature for 10 min, and immunostained with a primary antibody. For secondary reaction, an Alexa 488- or 568-labeled secondary antibody (Invitrogen) was used. Images were taken by TCS SP5 confocal microscope using an HCX PL APO 63X, 1.40 N.A., oil immersion objective lens (Leica) or FV1000D confocal microscope using a PL APO 60X, 1.35 N.A., oil immersion objective lens (Olympus).

Purification of Recombinant G0s2 Protein. The full-length mouse G0s2 cDNA was subcloned into pMAL-c2e (New England Biolabs), and then, the coding sequence of maltose-binding protein (MBP)-G0s2 was cloned into pET21a vector (pET21a-MBP-G0s2; Novagen). pET21a-MBP-G0s2 was transformed into BL21-Star (DE3; Invitrogen), and the expression of MBP-G0s2 protein was induced by the addition of 0.5 mM isopropyl β-D-1-thiogalactopyranoside. The cells were lysed by sonication, and the MBP-G0s2 protein was purified with amylose resin (New England Biolabs) followed by elution with the buffer (30 mM Mops, pH 7.5, 150 mM KCl, 0.01% *n*-dodecyl-β-D-maltoside, 20 mM maltose). The eluted protein was concentrated using Amicon Ultra-4 3K (Millipore) to remove maltose.

Pull-Down Assay. Preparation of submitochondrial particles from bovine heart mitochondria and subsequent purification of F_oF_1-ATP synthase were performed as described previously (2). Recombinant MBP fusion protein (4 μg) and purified F_oF_1-ATP synthase (16 μg) were incubated at 37 °C for 30 min in the presence of 1% CHAPS and then batch-bound to amylose resin at 4 °C for 1 h. After extensive washing, proteins were eluted with SDS/PAGE sample buffer.

Cell Viability. Cells (9×10^4) of cardiomyocytes seeded on 12-well plates were infected with adenovirus shRNA for 48 h or adenovirus LacZ or G0s2 for 24 h, and then, they were exposed to hypoxic condition for 18 h. Hypoxic condition (less than 0.1%) was achieved by using the AnaeroPack System (Mitsubishi Gas Chemical, Inc.). After hypoxia, cells were stained with 2 μg/mL propidium iodide (Sigma) and 2 μg/mL Hoechst 33342 (Dojin Chemical, Inc.) at 37 °C for 30 min. The stained nuclei were then visualized using a BZ-8000 Fluorescent Microscope (KEYENCE). Four fields in the plates (~400 cells per field) were counted, and data were expressed as percentage of propidium iodide-positive nuclei/total nuclei.

Measurement of ATP Synthesis Activity of Permeabilized Cells. ATP synthesis activities of HeLa cells were measured as described previously (3). Digitonin (50 μg/mL) was used to permeabilize the plasma membrane of cardiomyocytes.

Measurement of Intact Cellular Respiration. Oxygen consumption rate of cardiomyocytes was measured using an XF96 Extracellular Flux Analyzer (Seahorse Bioscience) in unbuffered DMEM assay medium supplemented with 1 mM pyruvate, 2 mM glutamate, and 25 mM glucose after 60 min equilibration according to the manufacturer's recommendations. The continuous measurements of oxygen consumption rate were collected over time under basal condition and in response to oligomycin A (1 μg/mL) and rotenone (100 nM) plus antimycin A (100 nM) or carbonyl cyanide-4-(trifluoromethoxy)-phenylhydrazone (0.5 μM).

Animals. All procedures were performed in conformity with the *Guide for the Care and Use of Laboratory Animals* (4) and approved by the Osaka University Committee for Laboratory Animal Use.

Statistical Analyses. Our data are expressed as means ± SEMs of at least three independent experiments. The two-tailed Student *t* test was used to analyze differences between two groups unless otherwise noted. $P < 0.05$ was considered statistically significant.

1. Seguchi O, et al. (2007) A cardiac myosin light chain kinase regulates sarcomere assembly in the vertebrate heart. *J Clin Invest* 117(10):2812–2824.
2. Chen R, Runswick MJ, Carroll J, Fearnley IM, Walker JE (2007) Association of two proteolipids of unknown function with ATP synthase from bovine heart mitochondria. *FEBS Lett* 581(17):3145–3148.
3. Fujikawa M, Yoshida M (2010) A sensitive, simple assay of mitochondrial ATP synthesis of cultured mammalian cells suitable for high-throughput analysis. *Biochem Biophys Res Commun* 401(4):538–543.
4. National Institutes of Health (1996) *Guide for the Care and Use of Laboratory Animals*, NIH Publication 85–23 (National Institutes of Health, Bethesda).

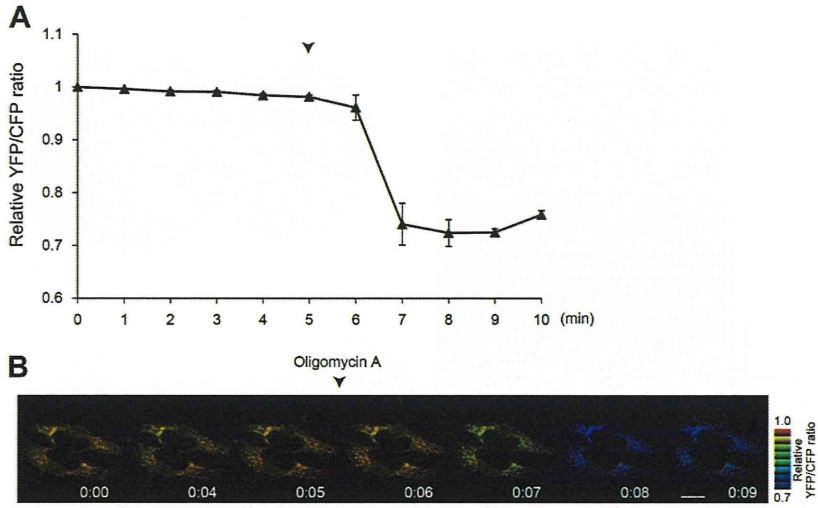

Fig. S1. Mit-ATeam assay is applicable in HeLa cells to assess oxidative phosphorylation activity. (*A*) YFP/CFP emission ratio plots of Mit-ATeam in HeLa cells. Oligomycin A (10 μg/mL) was added at 5 min (arrowhead; $n = 10$). All measurements were normalized to the YFP/CFP emission ratio at 0 min. Data are represented as the means ± SEMs. (*B*) Representative sequential YFP/CFP ratiometric pseudocolored images of Mit-ATeam in HeLa cells. Oligomycin A (10 μg/mL) was added at 5 min. (Scale bars: 20 μm.)

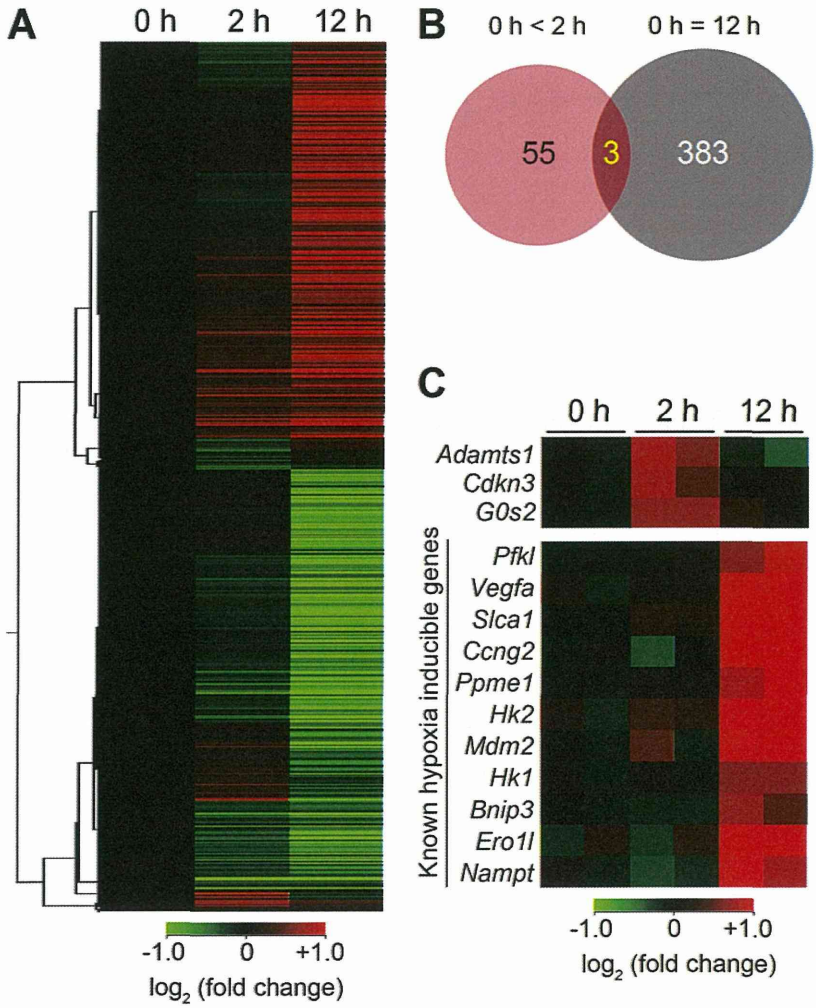

Fig. S2. Microarray analysis of hypoxia-treated cardiomyocytes and identification of *G0s2* as a rapidly inducible gene by hypoxia. (*A*) Hierarchical clustering image of 2,598 genes exhibiting significantly ($P < 0.05$; ANOVA) different expression levels at each of three time points (0, 2, and 12 h) measured in cardiomyocytes under hypoxic conditions (1% O_2). The red and green colors denote higher and lower levels of expression relative to the control sample (0 h), respectively. (*B*) Venn diagrams representing the overlap of genes that were up-regulated (>1.5-fold up-regulated) at 2 h and genes that remained unchanged (<1.2-fold change) after 12 h compared with the control at 0 h. (*C*) Heat map of the genes extracted from *A*. *Upper* shows the expression pattern of genes that were up-regulated at 2 h after the onset of hypoxia and declined to the baseline expression level at 12 h. *Lower* shows known hypoxia-inducible genes.

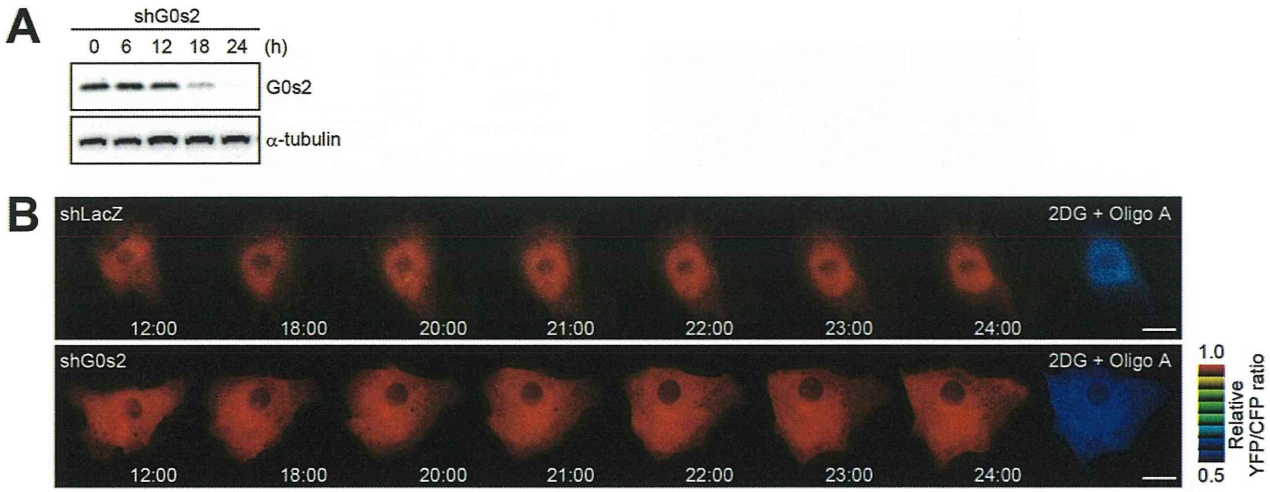

Fig. S3. G0s2 does not affect cytosolic ATP concentration. (*A*) Time course of G0s2 knockdown in cardiomyocytes. (*B*) Sequential YFP/CFP ratiometric pseudocolored images of Cyto-ATeam fluorescence in cardiomyocytes expressing shRNA for LacZ (shLacZ) or G0s2 (shG0s2; #2). Inhibitors of glycolysis [10 mM 2-deoxyglucose (2DG)] and F_oF_1-ATP synthase [1 μg/mL oligomycin A (Oligo A)] were added at the end of the time-lapse imaging to diminish the cytosolic ATP concentration. The indicated time represents the period after adenovirus infection.

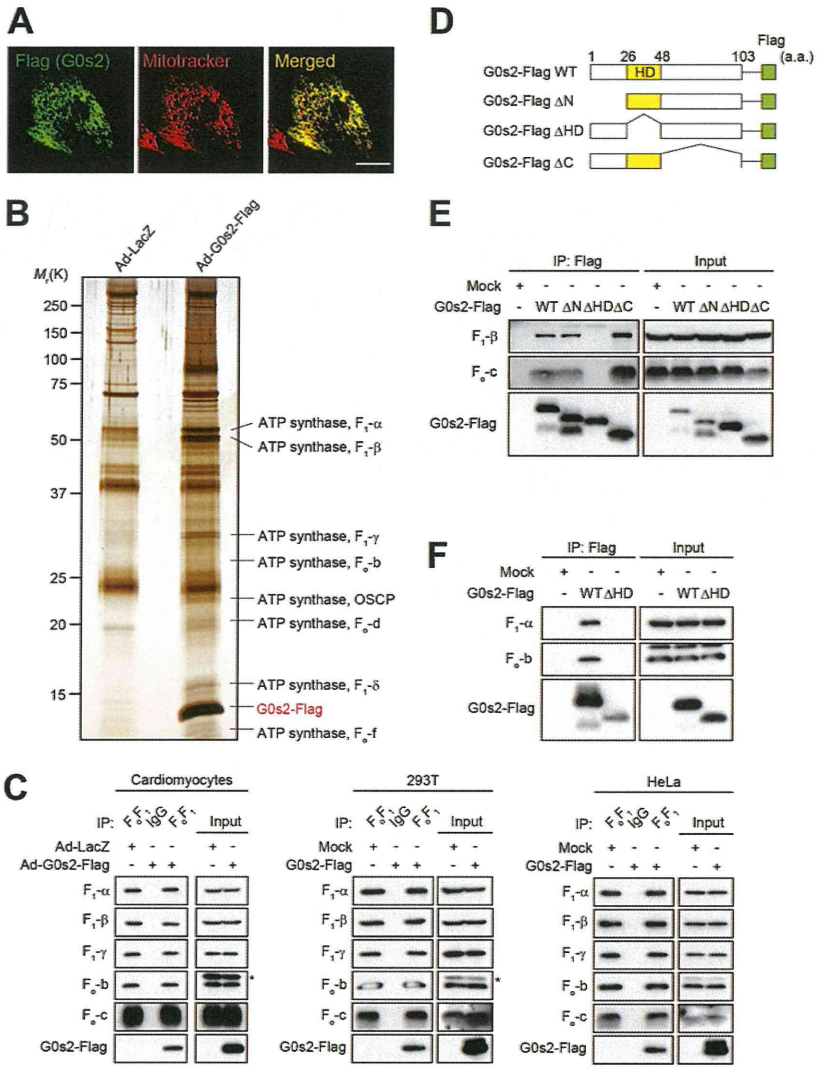

Fig. S4. Identification of F_oF_1-ATP synthase as the G0s2 binding protein. (*A*) Immunostaining of cardiomyocytes that expressed G0s2-Flag. The cells were stained with anti-Flag antibody (green) and labeled with MitoTracker Red (red). (Scale bar: 20 μm.) (*B*) A silver-stained gel of affinity-purified G0s2 binding proteins. Cell lysates from cardiomyocytes infected with adenovirus expressing G0s2-Flag or LacZ were purified with anti-Flag affinity gels. Polypeptides of the F_oF_1-ATP synthase complex identified by MS are indicated along with the G0s2-Flag protein (red). OSCP, oligomycin sensitivity conferral protein. (*C*) Immunoprecipitation (IP) of F_oF_1-ATP synthase in (*Left*) cardiomyocytes, (*Center*) 293T, and (*Right*) HeLa cells. F_oF_1, F_oF_1-ATP synthase. *Nonspecific band. (*D*) A schematic representation of the G0s2-Flag WT and deletion mutants. The hydrophobic domain (HD) of G0s2 is indicated as a yellow box. (*E* and *F*) IP of G0s2 mutants expressed in (*E*) 293T or (*F*) HeLa cells.